Purification and Properties of the Heme- and Iron−Sulfur-Containing Heterodisulfide Reductase from *Methanosarcina thermophila*†

Mihaela Simianu,‡ Eisuke Murakami,‡ John M. Brewer,§ and Stephen W. Ragsdale*,‡

Department of Biochemistry, The Beadle Center, University of Nebraska, Lincoln, Nebraska 68588-0664, and Department of Biochemistry and Molecular Biology, Life Sciences Building, University of Georgia, Athens, Georgia 30602-7229

Received October 24, 1997; Revised Manuscript Received May 13, 1998

ABSTRACT: The heterodisulfide reductase (HDR) from *Methanosarcina thermophila* was purified to homogeneity from acetate-grown cells. In the absence of detergents, HDR consisted of an eight-protein complex with hydrogenase activity. However, when HDR was purified in the presence of 0.6% Triton X-100, a two-subunit (53 and 27 kDa) high specific activity (∼200 units mg^{-1}) enzyme was obtained that lacked hydrogenase activity. Sedimentation equilibrium experiments demonstrated that HDR has a molecular mass of 206 kDa and a high partial specific volume (0.9 cm^3/g), indicating that the purified protein contains a significant amount of bound lipid. Like the HDR from *Methanosarcina barkeri* [Kunkel, A., Vaupel, M., Heim, S., Thauer, R. K., and Hedderich, R. (1997) *Eur. J. Biochem. 244*, 226−234], it was found to contain two discrete *b*-type hemes in the small subunit and two distinct $[Fe_4S_4]^{2+/1+}$ clusters in the large subunit. One heme is high-spin and has a high midpoint potential (−23 mV), whereas the other heme apparently is low-spin and exhibits a relatively low midpoint potential (−180 mV). Only the high-spin heme binds CO. The midpoint potentials for the two clusters are −100 and −400 mV. In the fully reduced state, a complicated EPR spectrum with *g* values of 2.03, 1.97, 1.92, and 1.88 was observed. This spectrum resembles that of 8Fe ferredoxins in the fully reduced state, indicating that the two clusters in HDR are near enough to experience relatively strong dipolar interactions. Kinetic studies in which CO oxidation is coupled to heterodisulfide reduction strongly indicate that a membrane-associated compound is the direct electron donor to HDR. An electron-transfer pathway is presented that postulates a mechanism for coupling electron transport to proton translocation.

The methanoarchaea are anaerobic microorganisms that synthesize methane from CO_2, formate, methanol, methylamines, or acetate. About 60−70% of the methane produced in nature results from the aceticlastic pathway of acetate metabolism by *Methanosarcina* and *Methanothrix* (*1*). Oxidation of the acetate carboxyl group to carbon dioxide provides the electrons to reduce the methyl group to methane. The first two steps in the aceticlastic pathway function to activate acetate to acetyl-CoA (*2, 3*). Then, a multienzyme complex containing CO dehydrogenase/acetyl-CoA synthase (CODH/ACS)[1] and a corrinoid iron−sulfur protein (CFeSP) disassemble acetyl-CoA to form methyltetrahydromethanopterin (methyl-H_4MPT), CO_2, and CoA (*4*−*9*). Next, a corrinoid containing methyltransferase transfers the methyl moiety from methyl-H_4MPT to coenzyme M (HS-CoM), forming methyl-CoM (*10*−*16*). Then, methyl-CoM reductase (MCR) catalyzes the reaction of methyl-CoM with 7-mercaptoheptanoyl-L-threonine phosphate (HS-HTP), which is also known as cofactor B (CoB-SH), to form methane and the heterodisulfide, CoM-S-S-CoB (eq 1) (*17*−*20*). Heterodisulfide reductase (HDR), which is the subject of this paper, regenerates HS-CoM and CoB-SH (*21*−*26*):

$$CH_3\text{-S-CoM} + \text{CoB-SH} \rightarrow CH_4 + \text{CoM-S-S-CoB} \quad (1)$$

$$\text{CoM-S-S-CoB} + 2H^+ + 2e^- \rightarrow \text{HS-CoM} + \text{CoB-SH} \quad (2)$$

Two classes of HDR have been purified and characterized. The first is from H_2/CO_2-grown cells of *Methanobacterium thermoautotrophicum* strain Marburg, which is a three-subunit protein containing FAD and iron−sulfur clusters (*21*). Based on sequence analysis, the large 80-kDa subunit was proposed to contain FAD, active site cysteine residues spaced in a similar motif to thioredoxin reductase, and four $[Fe_4S_4]$ clusters (*23*). The small 21-kDa subunit contains two sequence motifs that are characteristic of $[Fe_4S_4]$ clusters. The other class is a two-subunit HDR that was first isolated from methanol-grown cells of *Methanosarcina barkeri*. This

† Work described here was partially supported by DOE Grant ER20053 to S.W.R. The XL-A Analytical Ultracentrifuge was purchased with support from Grant BIR-9317749 to J.M.B. from the National Science Foundation.

* Address correspondence to this author at the Department of Biochemistry, The Beadle Center, University of Nebraska, Lincoln, NE 68588-0664. Phone: (402)-472-8912. FAX: (402)-472-7842. Email: sragsdal@unlinfo.unl.edu.

‡ University of Nebraska.

§ University of Georgia.

[1] Abbreviations: CODH/ACS, CO dehydrogenase/acetyl-CoA synthase; CFeSP, corrinoid iron−sulfur protein; Fd, ferredoxin; methyl-H_4MPT, methyltetrahydromethanopterin; HS-CoM, coenzyme M; MCR, methyl-CoM reductase; HDR, heterodisulfide reductase; CoB-SH, cofactor B; HS-HTP, 7-mercaptoheptanoyl-L-threonine phosphate; CoM-S-S-CoB, heterodisulfide of CoM and CoB; DTNB, 5,5′-dithiobis-(2-nitrobenzoate).

S0006-2960(97)02648-2 CCC: $15.00
Published on Web 06/18/1998

protein contains heme *b*, non-heme iron, and inorganic sulfide (*24*). DNA sequence analysis indicated the presence of two [Fe_4S_4] clusters in the 46 kDa subunit and heme in the 23-kDa subunit (*26*). The results described in this paper demonstrate that the *Ms. thermophila* HDR is a member of the heme iron−sulfur class such as the *Ms. barkeri* enzyme. Earlier, the *Ms. thermophila* HDR was enriched ∼2-fold from the soluble cell extract to a specific activity of 1.8 units mg^{-1} (*25*). We have purified the *Ms. thermophila* enzyme to homogeneity to a specific activity of 200 units mg^{-1} and shown that it contains (per heterodimeric unit) two distinct *b*-type hemes and two [Fe_4S_4] clusters.

The HDR reaction is coupled to the generation of an electrochemical ion gradient that is essential for energy conservation by methanogens. That proton translocation is coupled to electron transport pathways and ATP synthesis involving HDR-catalyzed heterodisulfide reduction was demonstrated when the electron donor was H_2 (*27*), CO (*28*), or reduced factor F_{420} (*29*). Factor F_{420} is a deazaflavin cofactor in methanogens that replaces pyridine nucleotides in other organisms. Two moles of protons is translocated per mole of heterodisulfide reduced (*29, 27*). In the CO-dependent system of *Ms. thermophila*, it was proposed that the electron-transfer pathway involves ferredoxin (Fd) reduction by CO and CODH and that reduced Fd then donates electrons to a membrane-bound electron-transfer chain including a Fd-dependent oxidoreductase and cytochrome *b* (*30*). Hydrogenases were considered to play a possible role in this electron-transfer pathway (*31*−*33*). To better understand the enzymatic mechanism of HDR, how electrons are transferred among the component metal centers in HDR to the heterodisulfide, and how electron transfer is linked to vectorial proton translocation, we have used spectroscopic and electrochemical methods to characterize the redox-active metal centers in HDR.

MATERIALS AND METHODS

Materials. Cofactor B was synthesized essentially as described (*34*, *35*). The *N*-hydroxysuccinimide ester of 7-methylthioheptanoic was coupled to L-threonine phosphate at 45 °C in the presence of sodium bicarbonate (*35*). The reaction product was purified on an Accell Plus QMA anion-exchange column (Waters) as described (*35*), except that the column was performed in the air to yield the homodisulfide, CoB-S-S-CoB. After the column was equilibrated with 50 mM ammonium bicarbonate, the reaction mix was loaded, and the column was washed successively with (i) the same buffer to elute hydroxysuccinimide, (ii) 0.1 M ammonium bicarbonate to remove other reaction byproducts, and (iii) 0.6 M ammonium bicarbonate to elute the homodisulfide. Next, the heterodisulfide was prepared from CoB-S-S-CoB and HS-CoM (Sigma) by a thiol−disulfide exchange reaction (*35*). The reaction mixture was then purified on a 10 × 250 mm Vydac C_{18} HPLC column that was developed with a linear gradient of 0−80% methanol in 25 mM ammonium bicarbonate, pH 3.3, at a flow rate of 2 mL min^{-1} for 30 min. The absorbance at 215 or 255 nm was monitored (*35*). The heterodisulfide eluted at 24 min in the gradient at 64% methanol, and it was determined to be 91% pure by ^1H NMR (*34*). Other chemicals were obtained from Sigma Chemical Co. and Aldrich Chemical Co., Inc.

Cell Growth and Enzyme Purification. Ms. thermophila strain TM-1 was cultured on acetate (*36*) in a 5 L BioFlow III pH-controlled fermentor at 50 °C, pH 6.8, with minimal agitation (50 rpm) for 8−10 days. The cells were harvested by decanting the medium to yield 100−150 g of cells (wet weight). Freshly harvested cells were transferred into a Vacuum Atmospheres anaerobic chamber and resuspended in either buffer A [50 mM Tris-HCl, pH 7.6, 10% (v/v) glycerol, 2 mM dithiothreitol, and 0.6% (v/v) Triton X-100] or buffer B [identical except that it contained 0.2% (v/v) Triton X-100 and the pH was 6.8]. The suspension was then sonicated for 15 min at 4 °C and centrifuged at 35 000 rpm for 2 h. HDR was purified from the supernatant. The membrane fraction was prepared by suspending the pellet in buffer A, centrifuging at 35 000 rpm for 1 h, and suspending the washed pellet in the same buffer.

When HDR was purified in buffer B (pH 7.6), the cell-free extract was applied to a 2.5 × 30 cm Q-Sepharose HP (Sigma) column that had been equilibrated with buffer B at a rate of 1 mL min^{-1}. The pH of buffer B during all purification steps was 7.6. The column was washed with 500−700 mL of this buffer and developed with a linear gradient from 0 to 0.84 M KCl. HDR activity was spread among several fractions. A fraction that eluted at ∼0.2 M KCl, containing 15% of the total activity, was used in further purification steps. This fraction also contained methyl viologen-reducing hydrogenase. HDR-containing fractions that eluted at 0.54, 0.62, and 0.75 M KCl also contained methyl-CoM reductase, CODH, and ferredoxin, respectively. The HDR-containing fraction that eluted at 0.2 M KCl was applied to a 2.5 × 15 cm Phenyl Sepharose HP column (Pharmacia) equilibrated with 0.7 M ammonium sulfate in buffer B and eluted with a linear gradient from 0.7 to 0 M ammonium sulfate. Fractions containing HDR activity eluted at ∼0.35 M ammonium sulfate. These fractions were pooled, concentrated to 4−6 mg mL^{-1} using a YM-30 membrane, and applied to a 2.5 × 50 cm Superose 6 (Pharmacia) molecular exclusion column that was equilibrated with 0.1 M KCl in buffer B and developed at a flow rate of 0.2−0.4 mL min^{-1}.

When HDR was purified in buffer A, the cell-free extract was applied to a 2.5 × 30 cm Q-Sepharose HP (Sigma) column equilibrated with buffer A (pH 7.6). The column was washed with 500−700 mL of this buffer, and ∼ 60% of the total HDR activity was eluted by washing with buffer A containing 0.1 M KCl. The active fractions were pooled, concentrated to 4−6 mg mL^{-1} using a YM-30 membrane, and applied to a 2.5 × 50 cm Superose 6 (Pharmacia) column, which was equilibrated with buffer A containing 0.1 M KCl and developed at 0.2−0.4 mL min^{-1}. When HDR was purified in buffer A, the Phenyl Sepharose step could be omitted.

CODH/ACS and Fd were also purified during the HDR preparation that was performed in buffer A. After eluting HDR, the Q Sepharose HP column was developed with a linear gradient from 0.1 to 0.8 M KCl in buffer A. CODH activity eluted at ∼0.5 M KCl and Fd at ∼0.8 M KCl. The CODH/ACS complex was further purified to homogeneity as previously described (*5*). The specific activity of CODH/ACS preparations used was between 200 and 300 μmol of CO oxidized min^{-1} mg^{-1} when measured at 56 °C using a CO-saturated buffer containing 50 mM Tris-HCl, pH 7.6, 2

mM DTT, and 10 mM methyl viologen. Ferredoxin preparations were purified (*32*) to ~90−94% homogeneity based on the ratio of the absorbance value at 390 nm to that at 280 nm (between 0.72 and 0.78). Fd preparations had a specific activity in the CO-dependent reduction of metronidazole (*31*) of 16.8 units/mg.

Enzyme Assays. HDR activity was measured at 56 °C by following the oxidation of reduced methyl viologen (*37, 38, 21, 22, 24, 25*). One unit of HDR activity is defined as 1 μmol of CoM-S-S-CoB reduced min^{-1}. Reconstitution of the CO−heterodisulfide oxidoreductase reaction was performed essentially as described earlier (*25*) at 50 °C in a stoppered 8-mL serum vial. The 1-mL reaction mixture contained 50 mM Tris-HCl, pH 7.6, 10% glycerol, 1 atm of CO, CODH/ACS (40 μg), Fd (1−100 μg), HDR (20 μg), and CoM-S-S-CoB (1.3 μmol). At different times, 25-μL samples were removed into a solution containing 0.1 mL of Ellman's reagent (1 mM DTNB in acetone) and 0.9 mL of 100 mM KP_i buffer, pH 8.2, and the amount of free thiol formed was measured at 412 nm. The value of the absorbance at 412 nm was an average of a minimum of five readings. A standard curve with varying concentrations of anaerobic HS-CoM was developed to calibrate the Ellman's reagent.

The H_2−heterodisulfide oxidoreductase activity was determined by monitoring the heme absorption intensity at 558 nm (*22*). Hydrogenase activity was measured at 56 °C with methyl viologen (*24*).

Protein was quantified using a Rose Bengal dye-binding method (*39*) with bovine serum albumin as standard. The protein concentration was also measured by total amino acid analysis and found to be nearly identical to that determined by the colorimetric determination. The purity was determined by SDS−polyacrylamide gel electrophoresis. The protein was visualized by silver (*40*) or Coomassie blue R-250 staining.

Amino Acid, Metal, and N-Terminal Sequence Analyses. The N-terminal amino acid sequence and the amino acid composition were performed at the Protein and Nucleic Acid Shared Facility of the Medical College of Wisconsin. The sequence was determined on a Beckman LF 3000G Peptide Sequencer. The sequence was analyzed with the Beckman 168DAD and system GOLD.

Iron was determined colorimetrically at 562 nm as a chelate with ferrozine and neocuproine (*41*) and by total iron analysis with bathophenanthroline (*42*). Acid-labile sulfur was determined spectrophotometrically at 670 nm as methylene blue using a freshly prepared $Na_2S-(H_2O)_9$ solution as a standard (*43*). Complete metal analysis was performed using the Jarrel-Ash 965 Atomcomp Plasma Emission Spectrograph at the Chemical Analysis Laboratory, University of Georgia, Athens.

The pyridine hemochrome of HDR was generated as described and compared with those of heme *a*, *b*, *c*, and *o* proteins (*44*−*46*). The heme was extracted in acid acetone and purified by HPLC on a C_{18} column by isocratic elution in ethanol/acetic acid/water at a ratio of 70:13:7 (*45*). The cytochrome *b* content was determined from the difference spectra of reduced − oxidized HDR at room temperature as described under Results. To determine which subunit contains heme, the subunits were separated at 4 °C by SDS−PAGE, and the polyacrylamide gels were stained for peroxidase activity with tetramethylbenzidine (*47*).

Spectroscopic and Spectroelectrochemical Methods. Electronic absorption spectra were acquired with a Beckman DU Series 7000 Diode Array Spectrophotometer or a Cary-14 Spectrophotometer modified by Olis (Bogart, GA). For low-temperature electronic absorption at 77 K, a dual-beam Aminco DW-2000TM UV−Visible Spectrophotometer equipped with a liquid nitrogen cooled cell was used.

To determine the midpoint potentials of the hemes, UV−visible spectroelectrochemistry was performed anaerobically at 20 °C in 100 mM Tris-HCl, pH 7, in a cell equipped with a gold wire working electrode, and silver/silver chloride reference and auxiliary electrodes (*48, 49*). Redox titrations were performed in both reductive and oxidative directions. All redox potentials are reported relative to the normal hydrogen electrode. The solution contained 5 μM HDR, 0.1 mM ferrocyanide ($E^{0'} = 0.408$V), 5 μM methylene blue ($E^{0'} = +0.011$ V), 8 μM indigotetrasulfonate ($E^{0'} = -0.046$ V), 8 μM indigodisulfonate ($E^{0'} = -0.125$ V), 20 μM anthraquinone 1,5-disulfonate ($E^{0'} = -0.174$ V), 20 μM anthraquinone 2-sulfonate ($E^{0'} = -0.225$ V), and 0.1 mM methyl viologen ($E^{0'} = -0.449$V) as redox mediators. To obtain clean spectra of HDR at different potentials without interference from the spectra of the mediators, the 300−800 nm spectrum of the enzyme equilibrated to a certain redox potential in the presence of the mediator dyes was first recorded with a Cary-14 spectrophotometer. Next, the spectrum of an identical dye mix in the absence of the protein was measured at the same redox potentials. The spectrum of the mediators was then subtracted from the spectrum of the protein sample at each potential. SpectraCalc software (Galactic Industries Co.) was used for all spectral data manipulations. The absorbance at 426 nm was followed to monitor heme reduction. The most oxidized heme spectrum was subtracted from all spectra acquired at lower redox potentials. This procedure was important because of the significant overlap between the 410-nm band of the oxidized heme and the 426-band of the reduced heme. Equilibrium was considered to be obtained when the measured potential drift was 2−3 mV in 5 min.

EPR spectroelectrochemical titrations were performed in a cell described previously (*50*) under a helium atmosphere. The redox states of the hemes and the Fe-S clusters were monitored by following the intensities of the EPR signals at *g* values of 6.2, 1.95, and 1.97. The titrations were performed at equilibrated potentials between +0.100 and −0.500 mV. The 10 μM HDR solution (total volume of 800−1000 μL) used for heme titration contained 0.1 mM ferrocyanide, 20 μM methylene blue, 20 μM indigotetrasulfonate, 20 μM indigodisulfonate, 20 μM anthraquinone 1,5-disulfonate, 20 μM anthraquinone 2-sulfonate, and 0.1 mM benzyl viologen ($E^{0'} = -0.358$ V) as redox mediators. For titrations at lower potentials, the dye mix also contained 0.1 mM methyl viologen, 0.1 mM 1,1′-trimethylene-2,2′-bipyridyl ($E^{0'} = -0.540$ V), and 0.1 mM 4,4′-dimethyl-1,1′-trimethylene-2,2′-dipyridyl ($E^{0'} = -0.586$ V). The EPR signals of the dyes were digitally subtracted from those of the protein.

Resonance Raman (RR) spectra were acquired in sealed spinning NMR tubes at room temperature using a Spex 1269 spectrometer with a Princeton Instruments ICCD-576 UV-

enhanced detector. The 406.6- and 413.1-nm excitation lines were provided by a Coherent Model Innova 100-K3 Krypton ion laser, and the 441.7-nm line was from a Linconix Model 4240 NB Helium Cadmium laser (10 mW at the sample). The spectra shown were obtained using a 413.1-nm excitation line, which is in preresonance with the Soret absorption. No improvement in the signal intensity was obtained with 406.6- or 441.7-nm excitation lines. The spectral data were analyzed using SpectraCalc software (Galactic Industries Co.). Both the high- and low-frequency spectra were calibrated with fenchone. The samples for RR spectroscopy contained about 150 μL of a 40 μM protein solution in buffer A. The optical spectrum of each sample was measured before and after RR spectroscopy on a HP 8452A Diode Array spectrophotometer.

Electron paramagnetic resonance (EPR) spectra were recorded on a Bruker ESP 300E EPR spectrometer equipped with a temperature controller (Oxford ITC4) and automatic frequency counter (Hewlett-Packard Co., Model 5340A). To determine the spin concentration, a 1 mM copper perchlorate standard solution was used. Prior to EPR spectroscopy, the samples were concentrated with a Microcon 30 membrane (Amicon) to 4−6 mg mL^{-1} HDR.

Molecular Mass Determinations. Determination of the molecular mass by size exclusion chromatography was performed on a Superose 6 column that had been calibrated using the molecular mass standards (Pharmacia) aldolase (158-kDa), catalase (232-kDa), ferritin (440-kDa), thyroglobulin (669-kDa), and blue dextran. Denaturing SDS−PAGE was performed as described (*4*).

Sedimentation equilibrium measurements were carried out using a Beckman Instruments Optima XLA Analytical Ultracentrifuge. To determine the molecular weight of a protein using sedimentation equilibrium, its partial specific volume is required (*51*). A partial specific volume of 0.745 cm^3/g HDR was calculated from the amino acid composition using the residue values of Perkins (*52*). This value would be inaccurate if HDR contains nonprotein components, such as lipid, or if it interacts extensively with constituents of the solvent (*51, 53, 54*). The molecular mass and true partial specific volume were determined by measuring the distribution of HDR in a centrifugal field in the presence of various mixtures of H_2O and D_2O (*53*) since H_2O and D_2O are thermodynamically identical. The effects of deuterium exchange on the molecular weight and partial specific volume in 40% and 80% D_2O were assumed to be described by factors (k) of 1.005 and 1.01 (*53, 54*), respectively. The solvent densities in 0, 40, and 80% D_2O were 1.025, 1.067, and 1.109 g/cm^3, respectively. The sedimentation equilibrium experiments utilized three double-sector cells and were carried out at various protein concentrations (typically 0.3−1.0 absorbance unit at 558 nm), rotor speeds of 8000−10 000 rpm, and at 20 °C. In each cell, 50−100 μL of buffer (50 mM Tris-HCl, pH 7.6, 10% glycerol, 0.6% Triton X-100, and 2 mM dithiothreitol) was loaded using gastight Hamilton syringes after repeatedly flushing the cells with argon. Migration of the protein was followed at 558 nm after 24 or 48 h. Since the use of a shorter solution column (50 μL) gave the same apparent molecular weight after 24 h, we concluded that the solutions were at equilibrium. Corrections for the solvent density were based on literature values (*55*). The data were fit to eq 3 using the Origins software supplied with the instrument (*56*).

Table 1: Purification of *M. thermophila* HDR

fraction	protein (mg)	activity (units)	specific activity (units/mg)	x-fold purification	yield (%)
cell-free extract (soluble fraction)	2145	2285	1.2		100
cell-free extract (membrane fraction)	430	170	0.4		
Q Sepharose HP	32	1536	48	40	59
Superose 6	5.7	1140	200	167	44

$$\frac{\text{slope of d(ln } c)/\text{d}(r^2)(\text{H}_2\text{O})}{\text{slope of d(ln } c)/\text{d}(r^2)(\text{H}_2\text{O})} = \frac{M(1 - V\rho\text{H}_2\text{O})}{kM(1 - V/k\rho\text{D}_2\text{O})} = \frac{M(1 - V\rho\text{H}_2\text{O})}{M(k - V\rho\text{D}_2\text{O})} \quad (3)$$

RESULTS

Purification and Physical Characterization of the Ms. thermophila HDR. HDR was purified from acetate-grown *Ms. thermophila* cells in buffers containing either 0.6% or 0.2% Triton X-100. Most of the activity was found in the soluble fraction. When 0.6% Triton X-100 was used in the cell lysis buffer, only 6−15% of the total activity was associated with membranes, and the specific activity ranged from 0.5 to 1.2 units mg^{-1}. Therefore, the HDR purification was only attempted from the soluble fraction.

The amount of detergent present during the purification procedure markedly affected the interaction between HDR and the other activities, such as hydrogenase. When HDR was purified in buffers containing 0.2% Triton X-100, HDR activity was found throughout the fractions from the chromatographic columns, apparently due to its association with other proteins. After three chromatographic steps, the resulting enzyme had been purified only 12-fold to a specific activity of 8 units mg^{-1}, and the methyl viologen-reducing hydrogenase was still present (7.3 units mg^{-1}). The product of this purification was a protein complex with an apparent molecular mass of 310 ± 10-kDa, based on gel exclusion chromatography. Analysis of the protein complex by SDS−PAGE (not shown) revealed a composition of eight subunits with molecular masses of 58, 47, 40, 28, 21, 18, 16, and 14-kDa. If these subunits were present in equal amounts, the total molecular mass would be 242-kDa. These results are similar to those reported for the H_2−heterodisulfide oxidoreductase complex isolated from membranes of *Ms. barkeri* (*38*). This complex contained, per milligram of protein, 1.6 nmol of heme *b*, 55 nmol of non-heme Fe, 55 nmol of acid-labile sulfide, 0.65 nmol of FAD, 23 mol of Zn, 4 mol of Cu, and 1.5 mol of Ni.

When HDR was purified in buffer A containing 0.6% Triton (Table 1), only two chromatographic steps were required to yield a homogeneous protein. Hydrophobic interaction chromatography on Phenyl Sepharose was omitted since it resulted in the loss of heme from the enzyme. After Superose 6 gel filtration chromatography, the HDR fractions had specific activities ranging from 160 to 230 units mg^{-1}. Analysis of the purified protein by SDS−PAGE revealed the presence of two subunits with apparent molecular masses of 53 and 27-kDa (Figure 1). Densitometric analysis of gels

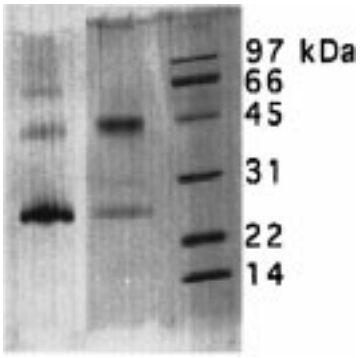

FIGURE 1: Analysis of the purified HDR by electrophoresis. Protein was denatured in SDS, separated at room temperature in 11% slab gels, and stained with Coomassie blue R250. Right lane: Molecular mass standards. Middle lane: HDR (2 μg) was boiled for 3 min in loading buffer containing 6% SDS. Left lane: To determine the subunit localization of the heme, HDR was incubated for 10 min at room temperature with 1% SDS denaturing buffer containing no mercaptoethanol before loading onto the 11% slab gel. The gel was run at 4 °C and stained for heme with 3,3′,5,5′-tetramethylbenzidine.

stained with either silver or Coomassie blue R250 revealed the optical density ratio of the two bands to be 4:1 (w/w), indicating that the subunit composition is $\alpha_2\beta$. However, since membrane proteins often exhibit anomalous staining intensities, we view this stoichiometry as tentative and have not ruled out the possibility that the composition is $\alpha\beta$. The studies reported below were performed with the two-subunit enzyme unless otherwise stated.

When HDR was chromatographed on a calibrated Superose 6 column, the apparent molecular mass was found to be 155 ± 20-kDa. Since its effective radius and not its molecular mass determines the migration of a protein during gel exclusion chromatography, sedimentation equilibrium experiments were performed. This method derives a size-independent or "pure" molecular mass (*51*). The molecular mass and the partial specific volume were determined by measuring the distribution of the 558-nm absorbance in solutions containing different amounts of D_2O. From three such measurements, V was measured to be 0.901 ± 0.015 $cm^3\ g^{-1}$ and the molecular mass was 206 000 ± 2100 Da. In each case, the data could be satisfactorily fit assuming a single thermodynamically ideal species after 24 h at 20 °C. The high value of the partial specific volume strongly suggests that HDR contains significant amounts of lipid. Since the partial specific volume of Triton X-100 is 0.919 cm^3/g (*55*), it is unlikely that the high partial specific volume is due to binding of Triton, since an unreasonably high percentage of Triton would have to be bound to produce a complex with such a partial specific volume. Further evidence for significant amounts of lipid in purified HDR samples includes tight binding of HDR to an Extracti-Gel D column (Pierce, Rockford, IL); the protein could only be eluted with ethanol. Further studies will be required to identify the nature of the bound lipid and to determine the relative proportions of lipid/protein in the purified enzyme.

The two subunits were subjected to N-terminal amino acid sequence analysis by the Edman degradation procedure (Figure 2). The N-terminal amino acid sequence of the 53-kDa subunit differed by only one residue from that of the large subunit (46 kDa) of the HDR from methanol-grown *Ms. barkeri.* The sequence of the 27-kDa subunit also showed high identity (three amino acids different) to the sequence of the 23-kDa subunit of the *Ms. barkeri* HDR.

```
Mt 53 KDA   AKRNPSIDTKNLTAVQLMEL
Mm 46 KDA   AKRTPSIDTKNLTAVQLMEL

Mt 27 KDA   SEEMVYFSGLSDALRITFVQ
Mb 23 KDA   SEEMLYFSGLSDVLRMTFVQ
```

FIGURE 2: N-terminal sequence comparison between the two HDR subunits from *Ms. thermophila* and *Ms. barkeri*.

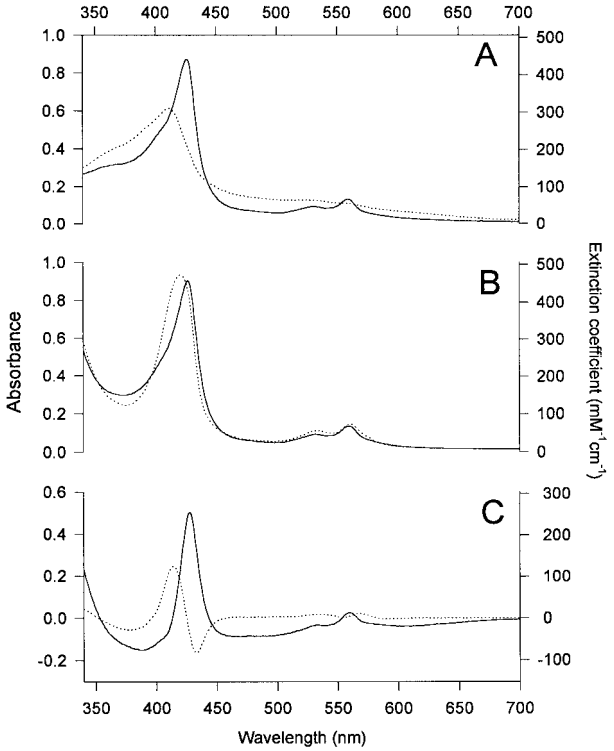

FIGURE 3: Room temperature spectra of purified HDR. Spectra were recorded with a Cary 14 spectrophotometer (modified by OLIS, Inc., Bogart, GA) using a 1-cm pathway cuvette under an N_2 atmosphere. The enzyme concentration was 2 μM ($\alpha\beta$ dimeric protein). (A) Solid line, HDR as-isolated; dotted line, oxidized by opening the solution to air. (B) Solid line, reduced by treating with a 50-fold excess of sodium dithionite; dotted line, CO adduct obtained by exposing a solution of reduced HDR to 1 atm of CO. (C) Solid line, difference spectra of dithionite-reduced minus oxidized; dotted line, difference spectrum of CO adduct minus dithionite-reduced. All extinction coefficients are based on a molecular mass of 80 kDa.

Characterization of the Cofactors. (A) Electronic Absorption Spectroscopy. Fractions containing HDR activity that were collected during the purification procedure exhibited an intense red−brown color and typical heme optical absorption spectra that intensified as the enzyme was purified. The as-isolated homogeneous enzyme in buffer A containing 2 mM dithiothreitol had a Soret absorption peak (the γ band) at 426 nm, an α band centered at 559 nm, and a β band at 531 nm (Figure 3A). These wavelength maxima are characteristic of cytochrome b_{558}. The electronic absorption spectral data in several ligation and redox states are summarized in Table 2. The Soret band was strongly asymmetric, indicating the existence of another chromophore that absorbs light in this region (see below). The α band is routinely used as an oxidation state marker for cytochrome *b*. Neither adding sodium dithionite (Figure 3B) nor electrochemically reducing the enzyme to −0.450 V significantly increased the α band intensity above that of the as-

Table 2: Spectral Properties of HDR

	band position, nm (ϵ, mM^{-1} cm^{-1})[a]		
state	Soret (γ)	β	α
reduced	426 (1120)	531 (107)	559 (156)
as-isolated	426 (1070)	531 (99)	559 (146)
oxidized	410 (695)		
red minus ox	max: 427 (682)		max: 559 (40)
	min: 463 (−104)		min: 577 (−52)
	max−min (787)		max−min (92)
red-CO	420 (1160)	533 (119)	561 (161)
red-CO minus red	max: 414 (310)		max: 567 (27)
	min1: 432 (−201)		min: 591 (−5)
	min2: 380 (−181)		max−min (32)
	max−min1 (511)		

[a] Based on a molecular mass of 206 kDa.

isolated enzyme, indicating that the heme was fully reduced. The intensities of the Soret and the α bands were used to determine the heme content. The extinction coefficients and metal compositions for HDR were based on the "pure" molecular mass determined by sedimentation equilibrium experiments. These extinction coefficients were then used to determine the heme content. Since the only chromophore that is expected to absorb in the 550-nm region is heme, the intensity of the α band was used to measure of the heme content. Based on the published ϵ for the α band of the ferrous heme, which ranges between 22.1 and 27 mM^{-1} cm^{-1} (*57*), the heme content was calculated to be 5.7−6.9 hemes per 206-kDa unit. This value would be equivalent to 2 hemes per $\alpha\beta$ dimeric protein; however, if the composition were instead $\alpha_2\beta$, the calculated value would be 4−5 hemes per trimeric unit.

When reducing agents were removed from the HDR solution, the Soret band exhibited a blue-shift to 410 nm and the α band at 559 nm disappeared (Figure 3A). Similar shifts occur when the Fe(II)-cytochrome b_{558} is oxidized to the ferric state. When HDR was oxidized with thionine, electrochemically oxidized, or treated with oxygen, the same optical spectrum was observed (not shown). No absorption bands in the 630−650-nm region were observed where many high-spin ferric hemes absorb. The difference spectrum of the reduced minus oxidized enzyme (Figure 3C) was nearly identical to that of cytochrome b_{558} (*37, 22, 24, 25*). The difference extinction coefficients ($\Delta\epsilon_{558-575}$) of reduced minus oxidized cytochrome *b* range between 17.5 and 19 mM^{-1} cm^{-1} (*58, 57*). Based on these values, the heme content was estimated to be 4.7−5.2 mol of heme *b* per 206-kDa unit, or approximately two *b*-hemes per dimeric unit.

When the optical absorption spectrum was obtained at liquid nitrogen temperatures (Figure 4), the asymmetry in the spectral region of the Soret bands of the reduced and oxidized enzymes was even more evident. The pronounced shoulders in the 390-nm region were characteristic of $[Fe_4S_4]$ proteins. The existence of FeS clusters was confirmed by EPR spectroscopy (see below). In the low-temperature difference spectrum (reduced minus oxidized), the α band was observed to split into two components with maximum absorption intensity at 555 and 559 nm (Figure 4, inset). The two bands had nearly equivalent intensities, strongly suggesting that approximately equal amounts of two distinct types of heme *b* were present. Similar results were obtained for the cytochrome *b*-containing membrane fraction from *Ms. barkeri* (*37*) and for the membrane-bound HDR from methanol-grown *Ms. barkeri* (*24*).

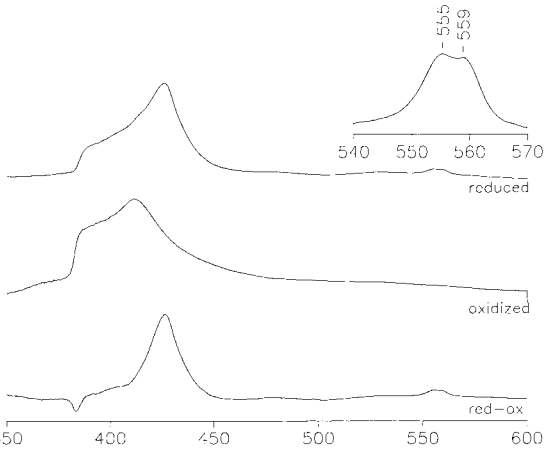

FIGURE 4: Low-temperature spectrum of HDR. Purified HDR (10 μM) in HDR buffer containing 60% glycerol was loaded anaerobically into a 2-mm quartz cuvette, and the same amount of buffer was loaded in the blank cuvette of the same holder. The cuvette holder was immersed in liquid nitrogen. Helium was slowly flowed over the solution to degas the dewar and avoid "the boiling" of liquid nitrogen. Top spectrum: HDR (as purified) dissolved in HDR buffer containing 60% glycerol at 77 K. Middle spectrum: The protein sample was removed from the cell, oxidized in air, and measured again at 77 K. Lower spectrum: The difference spectrum of (A) − (B). Inset: Focus on the region around the α band.

When as-isolated HDR was incubated with 1 atm of CO (∼0.8 mM in solution), there was a marked change in the optical spectrum (Figure 3B). A new Soret absorption band at ∼420 nm appeared that partially overlapped the 426-nm band. This shift is characteristic of the ferrous-CO adducts of *b*-type hemes, which have their γ bands in the 417−424-nm region (*59*). Deconvolution of the spectra revealed that the absolute intensities of the CO-bound and reduced hemes were present in equal intensity. The difference spectrum of CO-ligated minus as-isolated HDR (Figure 3C) revealed positive peaks at 414, 535, and 567 nm and a strong minimum at 432 nm. These features resemble those of CO-bound hemoglobin (*60*), myoglobin, and other heme *b*-containing proteins (*61*). The value for the maximum minus the minimum absorption values, $\Delta\epsilon_{414-380}$, was 511. Considering the analogous values for the CO adducts of myoglobin ($\Delta\epsilon_{417-370}$ = 177 mM^{-1} cm^{-1}) and hemoglobin ($\Delta\epsilon_{417-370}$ = 191 mM^{-1} cm^{-1} per heme), there are approximately two *b*-types hemes per 206-kDa unit that can bind CO, which is approximately half of the total *b*-heme present. The affinity of HDR for CO was further studied by adding small amounts of a CO-saturated buffer to the enzyme solution and measuring the difference spectra (Figure 5). The K_d for CO was found to be 0.8 μM (Figure 5, inset). These data strongly suggest that, even at CO concentrations 1000-fold higher than the K_d value, only one of the two *b*-type hemes in HDR binds CO. Presumably, there is one five-coordinate low-spin *b*-type heme that can bind CO and a hexacoordinate high-spin heme *b* that cannot.

The absorption spectrum of the pyridine hemochrome of HDR contained absorption peaks at 418, 522, and 554 nm (not shown). These peak positions were slightly blue-shifted relative to those of heme *b* in hemoglobin and myoglobin (at 419, 525, and 556 nm), determined under identical experimental conditions. A blue shift of similar magnitude

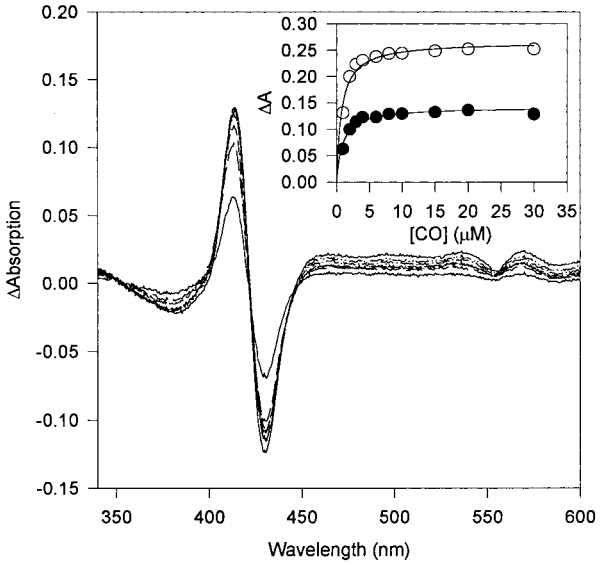

FIGURE 5: Titration of HDR with carbon monoxide. To determine to affinity of HDR for CO, 2 μM reduced HDR was titrated with CO by adding aliquots of a CO-saturated buffer (1 μM CO) into a cuvette containing 2 μM HDR in 1 mL. Final concentrations of CO were 1, 2, 3, 4, 6, 8, 10, 15, 20, and 30 μM. Each spectrum was subtracted from the reduced HDR spectrum. Inset: The difference absorption at 413 nm (●) and the sum of the difference absorption at 413 nm minus that at 430 nm ($\Delta A_{413-430}$) (○) were plotted against the CO concentration. The solid lines represent the fit of the data to the binding isotherm: $\Delta A = IC/(K_d + C)$, where I is the maximum difference absorption intensity at either 413 or 413−430 nm and C is the concentration of CO. The calculated K_d values for the ΔA_{413} and $\Delta A_{413-430}$ data were 0.8 ± 0.1 μM and 0.9 ± 0.1 μM, respectively.

was found in heme *o* of cytochrome *bo*, which has a more hydrophobic structure than heme *b* (*46*). However, after extracting the heme with acidic acetone, HPLC analysis revealed a single peak with a retention time that was identical to that of heme *b* extracted from hemoglobin. Therefore, HDR appears to contain only *b*-type hemes that are located in more hydrophobic environments than in hemoglobin. The hydrophobicity could have been provided by the protein or by the tightly bound lipid.

When SDS−PAGE gels were run at 4 °C under mildly denaturing conditions of either the eight-subunit complex (not shown) or the purified dimeric protein (Figure 1), the 27-kDa subunit stained for heme-derived peroxidase activity. There was a slight degree of peroxidase activity associated with the large subunit; however, this was much less than that of the small subunit, indicating that hemes are associated predominantly with the 27-kDa subunit. Possibly, the large subunit has a small degree of affinity for heme. This may indicate that the two subunits associate near the heme binding domain.

The purified protein was subjected to metal and acid-labile sulfide analyses (Table 3). The amount of iron in the sample was equivalent to 25−28 mol of Fe per 206-kDa unit. Since there are 5 hemes, this quantitates to 20−23 non-heme irons per dimeric protein, which is consistent with a composition of ~5 [Fe_4S_4] clusters per 206-kDa unit (see the EPR results, below). The amount of sulfide was slightly higher than the amount of iron, but is not inconsistent with the results of the iron analysis.

(B) Spectroelectrochemical Titration of HDR Monitored by UV−Visible Spectroscopy. Potentiometric titrations of

Table 3: Properties of the Purified *M. thermophila* HDR

apparent molecular mass (kDa)	155 ± 20 (gel exclusion chromatography)
	206 ± 2 (sedimentation equilibrium)
subunit mass (kDa)	53; 27
heme *b*	25 nmol mg^{-1};[a,b] 5.2 hemes mol^{-1}
total iron	135 ± 8 nmol mg^{-1}; 28 Fe mol^{-1} (*42*)
	120 ± 10 nmol mg^{-1};[a] 25 Fe mol^{-1} (plasma emission)
acid-labile sulfide	150 ± 20 nmol mg^{-1};[a] 31 sulfide mol^{-1}
EPR of reduced [Fe_4S_4]	26 ± 0.6 nmol of spins mg^{-1};[a] 5.4 spins mol^{-1}

[a] Based on a molecular mass of 206 kDa. [b] This is an average of the values determined by the red − ox and the CO − red difference spectra.

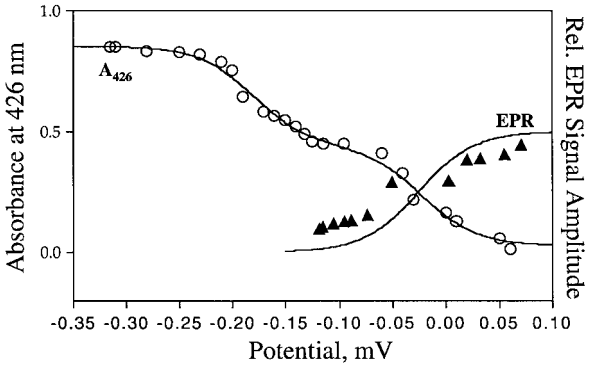

FIGURE 6: Spectroelectrochemical titration of the heme components of HDR. A solution containing 5 μM HDR was titrated by following the UV−visible absorption intensity at 426 nm at varied potentials. A 10 μM HDR solution was used in the EPR titrations, and the intensity of the $g \sim 6.0$ EPR signal was followed. The titrations were performed in the oxidative and reductive directions. Details of the titrations are provided under Materials and Methods.

HDR were monitored by optical spectroscopy (*48*). The intensity of the Soret absorption at 426 nm of the ferrous heme was used to determine the ratio of the oxidized/reduced heme at each measured potential. When the intensity of this peak was plotted against the redox potential, two separate redox processes with equal amplitudes were clearly evident (Figure 6). The experimental data were analyzed by a Nernst equation (eq 4) that relates the absorbance intensity at 426 nm to the redox potential for a process involving two one-electron reductions of a low-potential couple, E'_1, and a high-potential couple, E'_2. I represents the intensity of absorbance of the reduced heme, and n represents the number of electrons. The resulting midpoint potentials were $E'_1 = -0.180$ V and $E'_2 = -0.023$ V. Because the 558-nm absorbance is relatively weak, we were unable to follow the complete titration at that wavelength. Approximately half of the absorption of the α band decreased in each phase of the titration consistent with the conclusion that there are two types of *b*-type hemes that contribute equally to the absorption intensity in the Soret and the α-band regions.

$$I(E) = 0.44 + I/\{1 + \exp[(E - E'_1)n/0.0257]\} - I/\{1 + \exp[(E'_2 - E)n/0.0257]\} \quad (4)$$

(C) EPR Spectroscopic Studies of HDR. In the oxidized form of HDR and at temperatures below 10 K, a strong EPR signal was observed with g values at 6.22, 5.77, and 2.01 (Figure 7). These values are characteristic of high-spin ferric

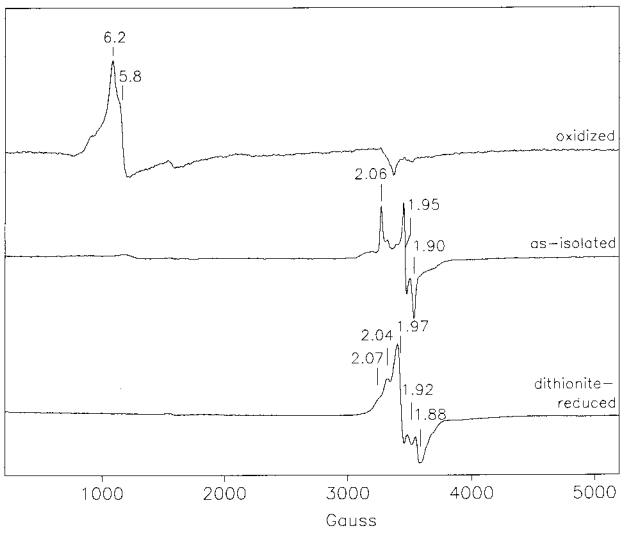

FIGURE 7: EPR spectra of HDR. Top spectrum: Oxidized HDR was obtained by treating HDR with thionine. EPR conditions: temperature, 5.4 K; power, 40 mW; microwave frequency, 9.4383 GHz; modulation amplitude, 10 G; modulation frequency, 100 kHz; gain, 20 000. Middle spectrum: as-isolated HDR in buffer A; EPR conditions were the same as just given except the frequency was 9.4364 GHz. Bottom spectrum: HDR was treated with 2 mM sodium dithionite; EPR conditions were the same except that the microwave frequency was 9.4378 GHz.

heme with ~3% rhombicity (*62*). Minor features were observed at g values of 7.3, 4.3, and ~3.2. The $g \sim 3.2$ feature, which is barely observable in this low-temperature spectrum, was studied in more detail since optical spectroscopic results indicate that the ferrous form of the enzyme contains a mixture of low- and high-spin hemes. There are many examples of low-spin hemes with g values at ~3.2, ~2.2, and ~1.5 (*62*). The intensity of the $g = 6.2$ component was greatest at temperatures below 9 K. As the temperature was increased, the $g = 6.2$ signal decreased in intensity as the $g \sim 3.2$ feature increased to an optimum between 13 and 17 K (not shown). However, even at its optimum temperature and over a wide range of microwave powers, we were unable to observe any partner for the 3.2 feature; the region around $g = 2.2$ was apparently devoid of EPR signals. This type of spectrum is called the "large g_{max}" type spectrum in which g_{max} is >3. Often the other two g values are not detected. This type of spectrum is frequently observed for hemes bound to two histidines or to histidine and methionine (*63*−*66*).

The trace in Figure 6 marked "EPR" corresponds to the electrochemical titration of the heme EPR signal at $g = 6.2$, which decreased in intensity as the redox potential was lowered. By the time the potential had been lowered to −70 mV, the $g = 6.2$ signal had completely disappeared. The solid line corresponds to the Nernst fit for a one-electron ($n = 1$) reduction of the high-spin heme center with a midpoint potential of −0.025 V, which is similar to that determined by UV−visible spectroelectrochemistry for the high-potential heme (above, $E = -0.023$ V). Therefore, the high-potential heme is in a high-spin state. It is puzzling that the UV−visible spectroelectrochemical titration showed the reduction of a second heme; however, we did not observe any strong ferric heme EPR signals at potentials more negative than −70 mV. Based on the RR results described below and the EPR results described above, the low-potential heme may be the low-spin heme that exhibits the $g = 3.2$ signal. Unfortunately, this signal was too weak to follow rigorously during the titration.

When HDR was air-oxidized (data not shown), the ferric heme EPR signals were unchanged; however, a new EPR signal appeared at a g value of 4.7, which probably results from adventitious iron, along with an intense $g = 2.02$ signal that is characteristic of a $[Fe_3S_4]$ cluster. These results indicate that exposure to oxygen decomposes the $[Fe_4S_4]$ clusters to the 3Fe state.

UV−visible (above) and RR (below) spectroscopic analyses of the as-isolated HDR indicated that the hemes were in an EPR-silent ferrous state. Therefore, the fully reduced enzyme should only exhibit EPR signals derived from the Fe-S clusters. The EPR spectrum of as-isolated HDR in buffer A (Figure 7) was dominated by a strong rhombic signal with g values at 2.06, 1.95, and 1.90, which could be observed at temperatures below 45 K. This signal will be referred to here as signal A. The intensities of the signals at each of these g values had identical temperature and power dependencies. The half-power of saturation ($P_{1/2}$) for signal A at 10 K was 7 mW, and at 20 K it was 15 mW. These properties are similar to those of the partially reduced 8Fe ferredoxins which contain a singly reduced and noninteracting $[Fe_4S_4]$ cluster in the 1+ oxidation state (*67*). Double integration of the spectrum in the $g = 2.0$ region relative to a copper perchlorate standard yielded a spin quantitation of 11.3−12.6 nmol of spins/mg of HDR. This corresponds to ~2.5 spins/mol, assuming a molecular mass of 206-kDa. Low-intensity features with g values at 2.11, 2.03, 1.97, and 1.76 were present along with some fast relaxing signals with g values of 8.2 and 5.6. As the temperature was decreased, the $g = 8.2$ and 5.6 signals increased in intensity, and at 10 K, none of these signals exhibited saturation at 200 mW power.

Reduction of HDR with dithionite markedly changed its EPR spectrum (Figure 7). The signals at $g = 8.2$ and 5.6 disappeared, and signal A was replaced by a complex spectrum with g values at 2.03, 1.97, 1.92, and 1.88, called signal B. The components of signal B had identical power and temperature dependencies with a $P_{1/2}$ at 10 K of 2 mW and at 20 K of 30 mW. Signal B could be observed at temperatures up to 60 K. Double integration of signal B yielded a spin integration of 3−5.4 spins/mol (assuming 206-kDa), or ~2 spins/mol of heterodimeric unit. The overall complex spectral morphology was highly similar to the spectrum of fully reduced 8Fe ferredoxins, which exhibit strong dipolar interactions due to the close proximity (within ~12 Å) of the two reduced $[Fe_4S_4]^{1+}$ (*67*).

The FeS clusters were further characterized by EPR spectroelectrochemical titrations between +0.100 and −0.500 V (Figure 8). Signal A followed a bell-shaped dependence on redox potential as best described by the Nernst equation (eq 5) for a one-electron reduction step with a midpoint potential of −0.100 V ($E1$) followed by a second one-electron reduction at a midpoint potential of −0.400 V ($E2$) (solid line). At low potentials, signal A decreased as signal B increased. The potential dependence of signal B was relatively poorly fit by eq 6 which describes a one-electron reduction with a midpoint potential of −0.450 V ($E3$) (dotted line). This type of redox behavior has been observed for 8Fe ferredoxins (*67*). This case would be like that of the

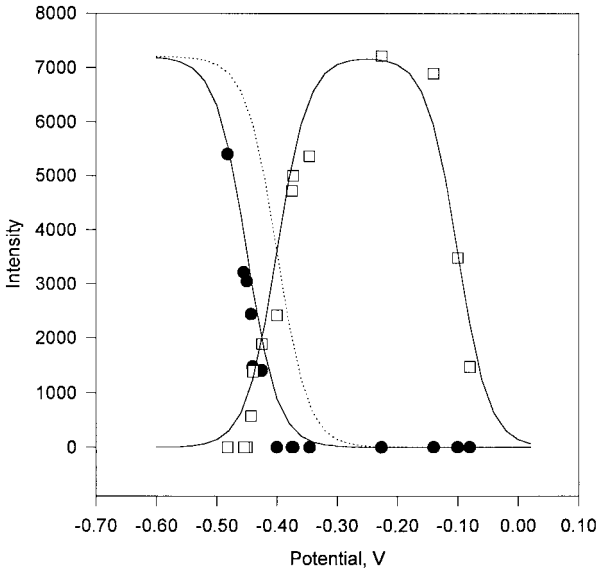

FIGURE 8: Redox titration of the FeS clusters of HDR. The intensities of signals A (□, singly reduced cluster) and B (●, both reduced clusters) were followed at varied potentials as described under Materials and Methods. The titrations were performed in the oxidative and reductive directions. The dotted line relates to the fit assuming that the interaction between the two clusters does not alter their apparent potential; the solid line relates to a fit that assumes that that they do.

clostridial ferredoxin in which interaction between the two $S = 1/2$ systems is strong enough to alter their EPR spectra but not strong enough to alter the redox potentials; therefore, the $E2$ and $E3$ values would be identical. A much better fit to the data could be obtained by allowing the values of $E2$ and $E3$ to differ as shown in Figure 8 (solid line), where the values of $E1$, $E2$, and $E3$ are −100, −400, and −450 mV, respectively. In this case, the two clusters would be expected to experience strong enough interactions to alter their redox potentials.

$$I = I_{max}/\{1 + \exp[(E1 - E)n/0.0257] + \exp[(E - E2)n/0.027]\} \quad (5)$$

$$I = I_{max}/\{1 + \exp[(E - E3)n/0.0257]\} \quad (6)$$

(D) RR Spectroscopy. The protein-bound hemes were further characterized by RR spectroscopy at room temperature with a 413.1-nm excitation line, which is in preresonance with the Soret absorption. The RR spectrum in the high-frequency region (1000−1700 cm^{-1}) contains information on the in-plane porphyrin vibrations, which are sensitive to iron coordination, spin, and oxidation state (*68*−*71*). The RR spectrum of HDR in this region was dominated by an intense symmetric peak at 1362 cm^{-1}, which is known as the ν_4 mode and can serve as the oxidation state marker for *b*-type hemes. The other high-frequency modes were much less resolved. The position of this mode provides strong evidence for a reduced heme structure in as-isolated HDR since, for model compounds and proteins containing heme *b*, this mode appears at ∼1376 cm^{-1} for the ferric and at ∼1360 cm^{-1} for the ferrous oxidation state (*68*). The ν_4 frequency in HDR is 3−5 cm^{-1} higher than that in high-spin ferrous histidine-coordinated heme proteins such as hemoglobin, myoglobin, and cytochrome *c* peroxidase (*69*) but identical to that of other *b*-cytochromes (*68*, *71*).

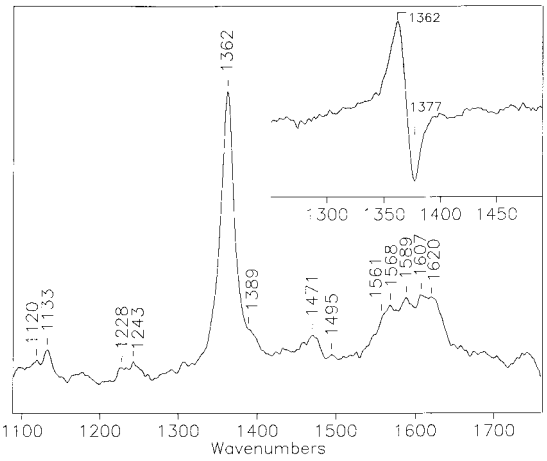

FIGURE 9: RR spectroscopy of reduced HDR. The high-frequency RR spectrum of 150 μL of 40 μM as-isolated HDR was obtained using a 413-nm excitation line and 10-mW power at the sample and acquired in a backscattering geometry. The total acquisition time was 10 min. The spectrum was base line corrected. Inset: Effect of CoB-SS-CoM on the heme oxidation state. The RR spectrum of the 40 μM HDR sample was recorded, and, after a 50-fold excess of CoB-S-S-CoM was added, another spectrum was recorded under the same conditions. The difference spectrum was obtained, and the region around the oxidation state marker band (ν_4 mode) was zoomed in. The maxima and the minima correspond to ratios of the ferrous/ferrous states.

Addition of CoM-S-S-CoB resulted in the appearance of a shoulder on the ν_4 mode at ∼1377 cm^{-1}, which indicates that the heme(s) undergo(es) partial oxidation upon addition of substrate. The shift of the oxidation state marker was much more noticeable in the difference spectrum (Figure 9, inset). The oxidation of HDR by CoM-S-S-CoB is further described below.

Longer accumulation times (8000 s) and subtraction of the white light spectrum from the absolute RR spectra improved the resolution of several "paired" frequencies in the region between 1500 and 1700 cm^{-1} that could be assigned to other marker modes (Figure 9) (*68*−*71*). Bands were observed at 1471 cm^{-1}, the ν_3 mode for high-spin pentacoordinate ferrous heme, and at 1494 cm^{-1}, which is the ν_3 mode for low-spin hexacoordinate Fe(II) heme. Another pair of bands was observed at 1568 cm^{-1}, the ν_2 mode for high-spin pentacoordinate Fe(II) heme, and at 1589 cm^{-1}, the ν_2 mode for low-spin hexacoordinate Fe(II) heme. In addition, vibrations at 1607 and 1620 cm^{-1}, which are the ν_{10} modes for high-spin pentacoordinate and low-spin hexacoordinate ferrous hemes, respectively, could be identified. Therefore, the RR spectrum of the reduced *b*-type heme in HDR apparently consists of a mixture of high-spin five-coordinate and low-spin six-coordinate ferrous hemes. Although the intensity of a Raman band depends on a number of parameters, the fact that the intensities of the pairs of ν_2, ν_3, and ν_{10} modes are nearly equivalent supports the hypothesis that HDR contains an equal mixture of high- and low-spin hemes in the reduced state.

Catalytic Properties. The HDR from *Ms. thermophila* catalyzed the reduction of CoM-S-S-CoB with reduced methyl or benzyl viologen. At saturating concentrations of heterodisulfide, the specific activity of the purified enzyme was 270 units mg^{-1} at 56 °C. The apparent K_m value for the heterodisulfide was 0.5 mM. It is of significant interest to replace the artificial dye mediators with the physiological

electron donor. Earlier, the CO-dependent reduction of CoM-S-S-CoB was measured in a reconstituted system from *Ms. thermophila* containing CODH, a 2-fold-enriched HDR fraction, Fd, and a membrane fraction containing cytochrome *b* (*25*). The membrane fraction was found to be absolutely essential for CO-dependent heterodisulfide reduction, and the rate increased with increasing Fd concentration. Based on these results, it was concluded that Fd transfers electrons from CODH to membrane-bound electron carriers, including cytochrome *b*, which acts as the electron donor for the final step in heterodisulfide reduction. When these experiments were performed, the HDR was impure, and it was not known that cytochrome *b* was a constituent of HDR (*25*). Thus, we performed similar reconstitution experiments using purified HDR, CODH/ACS complex, and Fd and monitored the rate of formation of HS-CoM and CoB-SH. In the absence of Fd, the generation of free thiols was not observed, even after 60 min of reaction. The rate was a linear function of Fd concentration (Figure 10A). Assuming a molecular mass for HDR of 206-kDa, the second-order rate constant could be calculated to be 2.0×10^5 M^{-1} s^{-1}. This is ~200-fold lower than the k_{cat}/K_m(Fd) for the CODH from *C. thermoaceticum* (*72*), in agreement with the conclusions of Peer et al. (*25*) that, although Fd is an efficient electron acceptor for CODH, it is not the physiological electron donor to HDR. Then, what is the physiological electron donor and where is it located? Addition of 10 μL (140 μg) of the membrane fraction increased the initial velocity by ~10-fold (Figure 10B). Since the activity of HDR in the membranes used in this experiment contained only 6% of the total HDR activity, i.e., 96% of the activity was supplied by the purified HDR, the results strongly indicate that the membrane fraction contains the direct physiological electron donor to HDR. Our results also demonstrate that no soluble electron carriers other than Fd are required to couple CODH to the membrane component(s).

Oxidation of reduced HDR by the heterodisulfide substrate was also determined by measuring the decrease in α band absorbance at 558 nm, and Fe-S cluster oxidation was measured under equilibrium conditions by EPR. Even at a 10^4-fold molar excess of heterodisulfide, only 42% of the heme and 38% of the FeS cluster underwent oxidation. Although, at equilibrium, only half of the hemes are oxidized, stopped-flow kinetic experiments have shown that both hemes undergo reduction by various electron donors at catalytically competent rates (Murakami and Ragsdale, unpublished results). Although these results indicate that the hemes undergo redox cycling during catalysis, ongoing kinetic experiments are required to evaluate the catalytic relevance of this oxidation state change.

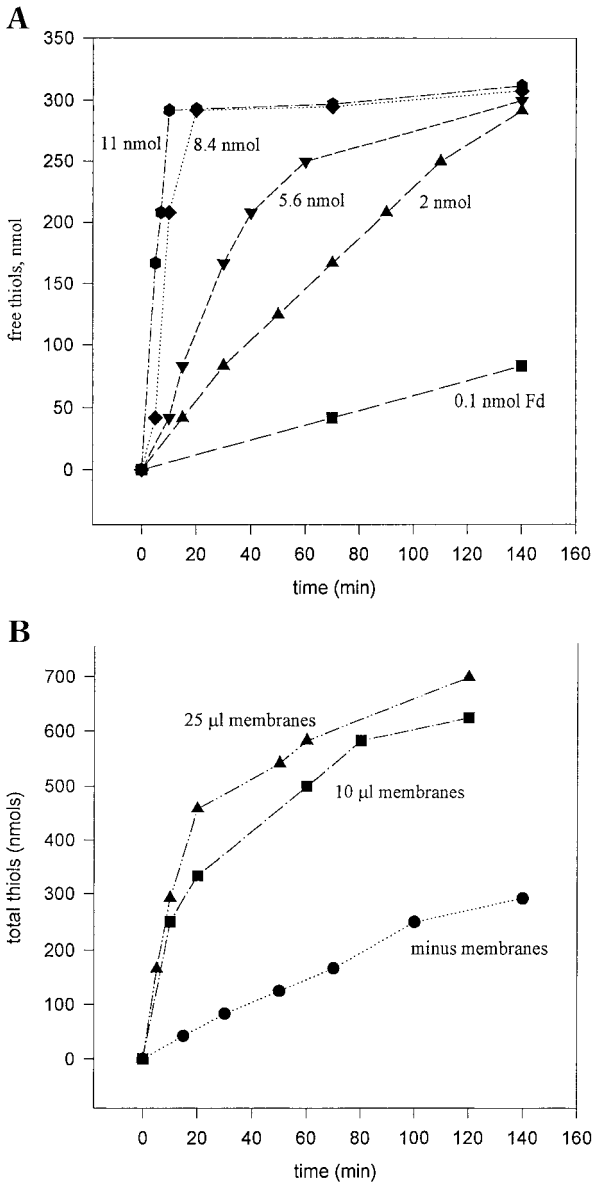

FIGURE 10: Reconstitution of CO:HDR activity. (A) Stimulation of HDR activity by Fd. Reduction of CoB-S-S-CoM by CO was performed at pH 7.6 and at 50 °C under similar conditions to those outlined earlier (*25*). The reaction mixture (described under Materials and Methods) contained CODH/ACS, HDR, and varying amounts of purified Fd, and the concentration of free thiols was determined with Ellman's reagent. (B) Effect of membrane fraction on CO:HDR activity. 10 or 25 μL of resuspended fresh membranes (14 mg/mL) was added to an assay mixture containing 15 μg of Fd and HDR as in (A), and the free thiols were determined by Ellman's reagent. Addition of 10 μL of membrane fraction increased the initial velocity from 70 to 625 nmol of CoB-S-S-CoB reduced min^{-1} (mg of HDR)$^{-1}$.

DISCUSSION

The catalytic challenge for HDR is that it contains redox cofactors that can accept and donate only one electron, yet it must perform two-electron reduction of the heterodisulfide substrate. A similar challenge faces proteins such as the plant ferredoxin:thioredoxin reductase. To understand the mechanisms of catalysis and electron transfer in the final steps of methanogenesis, we purified the thermostable HDR from *M. thermophila*, identified and characterized the component redox-active prosthetic groups, and performed some kinetic studies.

We purified the *Ms. thermophila* HDR to a specific activity of greater than 200 units mg^{-1}, which corresponds to a catalytic turnover number of ~270 s^{-1}, assuming that the enzyme contains two active sites per 206-kDa unit. Earlier preparations of HDR from different sources have had ~10-fold lower specific activities. One reason that this HDR is more active may be related to the higher cofactor content; for example, the purified *Ms. barkeri* protein contained 70% less heme (per milligram) (*26*) than the one studied here. Many properties of the *Ms. barkeri* (*26*) HDR are shared with the enzyme from *M. thermophila*. Both enzymes are

heterodimeric proteins with a ~50-kDa FeS-containing subunit and a ~25-kDa subunit containing heme *b*. Both enzymes lack flavin, in contrast to the HDR from *Mb. thermoautotrophicum*, which is a three-subunit enzyme with a subunit (HdrA) that contains FAD (*21*). The N-terminal sequences of the HDR subunits from *Ms. thermophila* and *Ms. barkeri* also are highly homologous. We expect that the additional properties described in this paper will also be shared.

It was found by sedimentation equilibrium analysis that the protein contains significant amounts of lipid. This property probably reflects a tight association of HDR with the cell membrane. Thauer proposed, based on DNA sequence analysis, that the small cytochrome *b*-containing subunit of the *Ms. barkeri* HDR is an integral membrane protein with five transmembrane-spanning helices and that the two *b* hemes are membrane-embedded (*26*). Our spectroscopic analyses indicate that the *Ms. thermophila* protein does indeed contain two *b*-type hemes that are located in a hydrophobic environment. The two hemes have vastly different redox potentials and different coordination environments. Based on the RR and CO binding experiments, it is likely that one of the hemes is low-spin and hexacoordinate (CO insensitive) while the other is high-spin and five-coordinate. Based on sequence analysis, it was earlier proposed that the *Ms. barkeri* enzyme contains one heme with bis-histidine and another with histidine and methionine ligands (*26*). Our spectroscopic results, however, indicate that there is one low-spin heme, which could correspond to either the bis-histidine- or the histidine-plus-methionine-coordinated heme, and, in addition, a high-spin heme with only one axial ligand.

Thauer et al. suggested that the *Ms. barkeri* iron−sulfur-containing subunit HdrD and the *Mb. thermoautotrophicum* HdrBC are structurally equivalent (*26*). They also proposed that, since flavin is not present in the catalytically active *Ms. barkeri* enzyme, neither the flavin subunit of the *Mb. thermoautotrophicum* HDR nor the cytochrome-containing subunit of the *Ms. barkeri* enzyme are involved in catalysis and that MbHdrD and MtHdrBC harbor the active sites of heterodisulfide reduction (*26*). However, we think that it is likely that the heme-containing subunit is a required component of HDR and that cytochrome and flavin may play analogous catalytic roles in the two systems. This is because the small subunit is tightly associated with HDR during the purification of the active enzyme and appears to be required for optimal activity. Occasionally we have purified relatively inactive preparations of HDR in which the small subunit is highly depleted. For example, one sample contained 0.02−0.05 heme/mol, had a small:large subunit ratio of ~1:20, and exhibited a specific activity of only 5 units mg^{-1} (i.e., approximately 2.5% of the standard activity). In addition, both hemes undergo reduction at catalytically competent rates (Murakami and Ragsdale, unpublished data).

Our working model of the CO:heterodisulfide oxidoreductase mechanism is shown in Figure 11. This scheme includes a possible explanation for how HDR can perform a two-electron reduction of RSSR to 2 mol of RSH when all of the redox sites in HDR are only capable of single-electron redox chemistry. It also proposes a mechanism for coupling electron transfer to proton translocation. First, CODH couples the reduction of Fd to the oxidation of CO, which

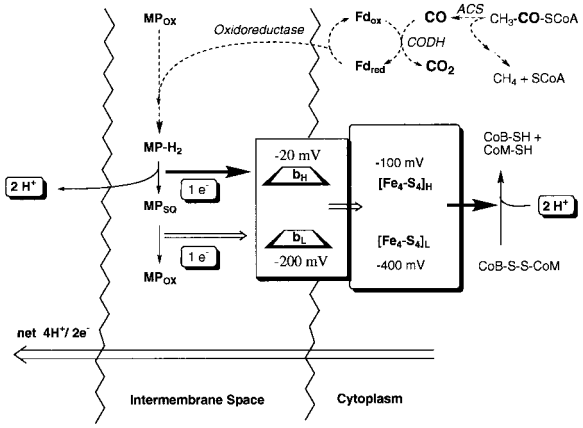

FIGURE 11: Scheme describing electron transport and proton translocation involving HDR. CODH, CO dehydrogenase; ACS, acetyl-CoA synthase; MP, methanophenazine. The midpoint potentials for the clusters are shown above or below the cartoons of the centers.

is derived from the disassembly of acetyl-CoA by acetyl-CoA synthase. Based on the kinetic experiments described here, we think that it is highly unlikely that Fd can serve as the physiological direct electron donor to HDR. Our results combined with those of Peer et al. (*25*) clearly demonstrate that the direct electron donor is a membrane component. This reductant could be methanophenazine, which has recently been isolated from membranes of methanol-grown cells of *Ms. mazei* (*73*). Attempts have not been made to isolate methanophenazine from the membranes of acetate-grown cells; however, recent studies have shown that it can directly reduce HDR (*74*). Further studies are required to understand the pathway of electron flow from the membrane component to the heterodisulfide in acetoclastic methanogenesis. The redox properties of phenazine are similar to those of quinones. Like cytochrome bc_1, for which detailed structural information is now available (*75*), this reaction could occur through two- or one-electron steps. In cytochrome bc_1, the first one-electron-transfer step appears to be coupled to the extrusion of two protons. Since the cytochrome-containing subunit is membrane-associated (*26*), it appears likely that the initial steps of electron transfer to HDR may occur to the cytochromes, as shown in Figure 11. On the other hand, the thermodynamically most favorable sequence would be as shown in eq 7:

$$\text{Phen-H}_2 \rightarrow \text{FeS}_L \rightarrow b_L \rightarrow \text{FeS}_H \rightarrow b_H \qquad (7)$$

We propose that the FeS-cluster-containing subunit accepts electrons from the heme subunit and acts as the direct electron donor to the heterodisulfide substrate. One reason for this hypothesis is that this subunit appears to be located in the cytoplasm (*26*) where the heterodisulfide would be located. A problem that HDR must overcome is that the cluster can only transfer one electron at a time, whereas the heterodisulfide substrate requires two-electron reduction. Possibly disulfide reduction occurs in two steps—the first would generate a thiyl radical, and the second would produce the two-electron-reduced product. For this to be feasible, there would have to be a mechanism of stabilizing the typically highly unstable sulfur radical. Johnson et al. proposed a model for the plant ferredoxin:thioredoxin reductase that may be relevant to HDR in which the thiyl

radical is stabilized by covalent attachment to a [Fe_4S_4] cluster (*76*). Possibly, for HDR, one of the two FeS clusters transfers electrons and directly interacts with the heterodisulfide substrate. Interaction between the reduced low-potential FeS cluster and the heterodisulfide substrate would be expected to make the apparent midpoint potential of the cluster more positive and that of the heterodisulfide more negative. Important tests of this hypothesis will include performing redox titrations of HDR in the presence of substrates and rapid kinetic experiments to trace electron flow among the component redox centers.

ACKNOWLEDGMENT

We thank Professor Tom Elthon (Biology Department, University of Nebraska, Lincoln, NE) for sharing his Aminco spectrophotometer for low-temperature UV−visible measurements and Jim Kincaid (Marquette University, Milwaukee, WI) for allowing the use of his Resonance Raman Spectrometer.

REFERENCES

1. Ferry, J. G., Ed. (1993) in *Methanogenesis: ecology physiology, biochemistry & genetics*, p 536, Chapman & Hall, London.
2. Aceti, D. J., and Ferry, J. G. (1988) *J. Biol. Chem. 263*, 15444−15448.
3. Fisher, R., and Thauer, R. K. (1988) *FEBS Lett. 228*, 249−253.
4. Laemmli, U. K. (1971) *Nature (London) 227*, 680−685.
5. Terlesky, K. C., Nelson, M. J. K., and Ferry, J. G. (1986) *J. Bacteriol. 168*, 1053−1058.
6. Abbanat, D. R., and Ferry, J. G. (1991) *Proc. Natl. Acad. Sci. U.S.A. 88*, 3272−3276.
7. Raybuck, S. A., Ramer, S. E., Abbanat, D. R., Peters, J. W., Orme-Johnson, W. H., Ferry, J. G., and Walsh, C. T. (1991) *J. Bacteriol. 173*, 929−932.
8. Lu, W.-P., Jablonski, P. E., Rasche, M., Ferry, J. G., and Ragsdale, S. W. (1994) *J. Biol. Chem. 269*, 9736−9742.
9. Grahame, D. A., and Demoll, E. (1996) *J. Biol. Chem. 271*, 8352−8358.
10. Becher, B., Müller, V., and Gottschalk, G. (1992) *J. Bacteriol. 174*, 7656−7660.
11. Gärtner, P., Ecker, A., Fischer, R., Linder, D., Fuchs, G., and Thauer, R. K. (1993) *Eur. J. Biochem. 213*, 537−545.
12. Gartner, P., Weiss, D. S., Harms, U., and Thauer, R. K. (1994) *Eur. J. Biochem. 226*, 465−472.
13. Harms, U., Weiss, D. S., Gartner, P., Linder, D., and Thauer, R. K. (1995) *Eur. J. Biochem. 228*, 640−648.
14. Lu, W.-P., Becher, B., Gottschalk, G., and Ragsdale, S. W. (1995) *J. Bacteriol. 177*, 2245−2250.
15. Harms, U., and Thauer, R. K. (1996) *Eur. J. Biochem. 235*, 653−659.
16. Lienard, T., Becher, B., Marschall, M., Bowien, S., and Gottschalk, G. (1996) *Eur. J. Biochem. 239*, 857−864.
17. Jablonski, P. E., and Ferry, J. G. (1991) *J. Bacteriol. 173*, 2481−2487.
18. Bonacker, L. G., Baudner, S., Mörschel, E., Böcher, R., and Thauer, R. K. (1993) *Eur. J. Biochem. 217*, 587−595.
19. Kuhner, C. H., Lindenbach, B. D., and Wolfe, R. S. (1993) *J. Bacteriol. 175*, 3195−3203.
20. Goubeaud, M., Schreiner, G., and Thauer, R. K. (1997) *Eur. J. Biochem. 243*, 110−114.
21. Hedderich, R., Berkessel, A., and Thauer, R. K. (1990) *Eur. J. Biochem. 193*, 255−261.
22. Heiden, S., Hedderich, R., Setzke, E., and Thauer, R. K. (1993) *Eur. J. Biochem. 213*, 529−535.
23. Hedderich, R., Koch, J., Linder, D., and Thauer, R. K. (1994) *Eur. J. Biochem. 225*, 253−261.
24. Heiden, S., Hedderich, R., Setzke, E., and Thauer, R. K. (1994) *Eur. J. Biochem. 221*, 855−861.
25. Peer, C. W., Painter, M. H., Rasche, M. E., and Ferry, J. G. (1994) *J. Bacteriol. 176*, 6974−6979.
26. Kunkel, A., Vaupel, M., Heim, S., Thauer, R. K., and Hedderich, R. (1997) *Eur. J. Biochem. 244*, 226−234.
27. Deppenmeier, U., Blaut, M., and Gottschalk, G. (1991) *Arch. Microbiol. 155*, 272−277.
28. Deppenmeier, U., Muller, V., and Gottschalk, G. (1996) *Arch. Microbiol. 165*, 149−163.
29. Deppenmeier, U., Blaut, M., Mahlmann, A., and Gottschalk, G. (1990) *Proc. Natl. Acad. Sci. U.S.A. 87*, 9449−9453.
30. Latimer, M. T., Painter, M. H., and Ferry, J. G. (1996) *J. Biol. Chem. 271*, 24023−24028.
31. Terlesky, K. C., and Ferry, J. G. (1988) *J. Biol. Chem. 263*, 4075−4079.
32. Terlesky, K. C., and Ferry, J. G. (1988) *J. Biol. Chem. 263*, 4080−4082.
33. Daas, P. J. H., Hagen, W. R., Keltjens, J. T., and Vogels, G. D. (1994) *FEBS Lett. 356*, 342−344.
34. Noll, K. M., Rinehart, K. L., Jr., Tanner, R. S., and Wolfe, R. S. (1986) *Proc. Natl. Acad. Sci. U.S.A. 83*, 4238−4242.
35. Noll, K. M., Donnelly, M. I., and Wolfe, R. S. (1987) *J. Biol. Chem. 262*, 513−515.
36. Ahring, B. K., Mondragon, F. A., Westermann, P., and Mah, R. A. (1991) *Appl. Microbiol. Biotechnol. 35*, 686−689.
37. Kuhn, W., and Gottschalk, G. (1983) *Eur. J. Biochem. 135*, 89−94.
38. Hedderich, R., Berkessel, A., and Thauer, R. K. (1989) *FEBS Lett. 255*, 67−71.
39. Elliott, J. I., and Brewer, J. M. (1978) *Arch. Biochem. Biophys. 190*, 351−357.
40. Morrissey, J. H. (1981) *Anal. Biochem. 117*, 307−310.
41. Fish, W. W. (1988) *Methods Enzymol. 158*, 357−364.
42. Doeg, K. A., and Ziegler, D. M. (1962) *Arch. Biochem. Biophys 97*, 37−40.
43. Cline, J. D. (1969) *Limnol. Oceanogr. 14*, 454−458.
44. Falk, J. E. (1975) in *Porphyrins and Metalloporphyrins*, Elsevier Scientific Publishing Co., New York.
45. Berry, E. A., and Trumpower, B. L. (1987) *Anal. Biochem. 161*, 1−15.
46. Puustinen, A., and Wikstrom, M. (1991) *Proc. Natl. Acad. Sci. U.S.A. 88*, 6122−6126.
47. Thomas, P. E., Ryan, D., and Levin, W. (1976) *Anal. Biochem. 75*, 169−170.
48. Dutton, L. (1978) *Methods Enzymol. 54E*, 411−435.
49. Stankovich, M. T. (1980) *Anal. Biochem. 109*, 295−308.
50. Harder, S. A., Feinberg, B. F., and Ragsdale, S. W. (1989) *Anal. Biochem. 181*, 283−287.
51. Tanford, C. (1961) in *Physical Chemistry of Macromolecules*, Wiley and Sons, New York.
52. Perkins, S. J. (1986) *Eur. J. Biochem. 157*, 169−180.
53. Edelstein, S. J., and Schachman, H. K. (1967) *J. Biol. Chem. 242*, 306−311.
54. Fless, G. M., and Santiago, J. Y. (1997) *Biochemistry 36*, 223−238.
55. Durschlag, H. (1986) in *Thermodynamic Data for Biochemistry and Molecular Biology*, Springer-Verlag, Berlin.
56. McRorie, D. K., and Voelker, P. J. (1993) in *Self-Associating Systems in the Analytical Ultracentrifuge*, Spinco Division of Beckman Instruments, Inc., Palo Alto, CA.
57. Weiss, H., and Ziganke, B. (1978) *Methods Enzymol. 53*, 212−221.
58. Deeb, S. S., and Hager, L. P. (1964) *J. Biol. Chem. 239*, 1024−1031.
59. Woods, P. M. (1984) *Biochim. Biophys. Acta 768*, 293−317.
60. Eaton, W. A., and Hofrichter, J. (1981) *Methods Enzymol. 76*, 175−261.
61. Wood, P. M. (1984) *Biochim. Biophys. Acta 768*, 293−317.
62. Blumberg, W. E., and Peisach, J. (1971) in *Probes of Structure and Function of Macromolecules and Membranes: Probes of Enzymes and Hemoproteins* (Chance, B., Yonetani, T., & Mildvan, A. S., Eds.) Vol. 2, pp 215−229, Academic Press, New York.

63. Taylor, C. P. S. (1977) *Biochim. Biophys. Acta 491*, 137−149.
64. Walsh, T. A., Johnson, M. K., Thomson, A. J., Barber, D., and Greenwood, C. (1981) *J. Inorg. Biochem. 14*, 1−14.
65. Spinner, F., Cheesman, M. R., Thomson, A. J., Kaysser, T., Gennis, R. B., Peng, Q., and Peterson, J. (1995) *Biochem. J. 308*, 641−644.
66. Cheesman, M. R., Ferguson, S. J., Moir, J. W., Richardson, D. J., Zumft, W. G., and Thomson, A. J. (1997) *Biochemistry 36*, 16267−16276.
67. Prince, R. C., and Adams, M. W. W. (1987) *J. Biol. Chem. 262*, 5125−5128.
68. Hurst, J. K., Loehr, T. M., Curnutte, J. T., and Rosen, H. (1991) *J. Biol. Chem. 266*, 1627−1634.
69. Sun, J., Wilks, A., Ortiz de Montellano, P. R., and Loehr, T. M. (1993) *Biochemistry 32*, 14151−14157.
70. Sun, J., Osborne, J. P., Kahlow, M. A., Kaysser, T. M., Gennis, R. B., and Loehr, T. M. (1995) *Biochemistry 34*, 12144−12151.
71. Vartosis, C., Babcock, G. T., Horsman, J. A. G., and Gennis, R. B. (1995) *J. Phys. Chem. 99*, 16817−16820.
72. Seravalli, J., Kumar, M., Lu, W.-P., and Ragsdale, S. W. (1997) *Biochemistry 36*, 11241−11251.
73. Abken, H. J., Tietze, M., Brodersen, J., Bäumer, S., Beifuss, U., and Deppenmeier, U. (1998) *J. Bacteriol.* (in press).
74. Baeumer, S., Murakami, E., Brodersen, J., Gottschalk, G., Ragsdale, S., and Deppenmeier, U. (1998) *FEBS Lett.* (in press).
75. Xia, D., Yu, C. A., Kim, H., Xian, J. Z., Kachurin, A. M., Zhang, L., Yu, L., and Deisenhofer, J. (1997) *Science 277*, 60−66.
76. Staples, C. R., Ameyibor, E., Fu, W. G., Gardetsalvi, L., Strittetter, A. L., Schurmann, P., Knaff, D. B., and Johnson, M. K. (1996) *Biochemistry 35*, 11425−11434.

BI9726483